

ORBITAL STABILITY AND PRECESSION EFFECTS IN THE KEPLER-89 SYSTEM

STEPHEN R. KANE

Department of Earth and Planetary Sciences, University of California, Riverside, CA 92521, USA

ABSTRACT

Among the numerous discoveries resulting from the *Kepler* mission are a plethora of compact planetary systems that provide deep insights into planet formation theories. The architecture of such compact systems also produces unique opportunities to study orbital dynamics in compact environments and the subsequent evolution of orbital parameters. One of the compact *Kepler* systems is Kepler-89; a system for which the radial velocity follow-up observations place strong upper limits on the masses of the planets and their Keplerian orbital elements. The potential for non-circular orbits in this system make it a compelling system to study dynamical constraints on the measured orbital parameters. We present a dynamical analysis of the system that demonstrates the stability of the circular model and shows the eccentric model of the system is not stable. The analysis indicates that planets c and d, although close to the 2:1 secular resonance, do not permanently occupy the 2:1 resonance configuration. We explore regions of orbital parameter space to identify the upper bounds of orbital eccentricity for the planets. We further show how the dynamics in the compact system leads to significant periastron precession of the innermost planets. Finally, we quantify the effect of the periastron precession on the transit times of the planets compared with the cyclic variations expected from transit timing variations.

Keywords: planets and satellites: dynamical evolution and stability – planetary systems – stars: individual (Kepler-89)

1. INTRODUCTION

The escalation in exoplanet discoveries have revealed a large diversity in planetary system architectures, many of which are substantially different to the architecture of our Solar System (Winn & Fabrycky 2015). The kinds of architectures being unveiled are largely being driven by the observational biases towards relatively small star–planet separation, such as those biases intrinsic to the transit method (Kane & von Braun 2008). For example, the discovery of many compact planetary systems have primarily resulted from the observations by *Kepler* (Borucki et al. 2010; Borucki 2016) and *K2* (Howell et al. 2014). An early example of such a compact system is that of Kepler-11, currently known to have at least six low density planets orbiting the host star (Lissauer et al. 2011, 2013). Many of these compact planetary systems have also been found to manifest signatures of gravitational interactions in the form of transit timing variations (TTVs) (Holman et al. 2010; Holczer et al. 2016). Such compact systems are enticing case studies for dynamical interactions between plan-

ets and their long-term stability (Funk et al. 2010; Kane 2015; Quarles et al. 2017; Granados Contreras & Boley 2018) as well as the stability of exomoon companions (Kane 2017).

The Kepler-89 (KOI-94) system is a good example of a compact system and consists of four planets with orbital periods in the range of 3.74–54.32 days (Weiss et al. 2013). The inner planet is a large terrestrial planet with a measured density of $10.1 \pm 5.5 \text{ g/cm}^{-3}$ whilst the outer planets are gas giants with densities $< 1 \text{ g/cm}^{-3}$. A combined fit of Keck/HIRES radial velocity (RV) observations and *Kepler* photometry by Weiss et al. (2013), combined with a TTV analysis by Masuda et al. (2013), yielded an orbital solution with Keplerian components. The possibility of non-zero eccentricities introduces significantly more dynamical interactions between the planets and the potential for regions of instability within the orbital parameter space. Additionally, the impact of these planetary interactions may result in precession of the orbits that would impact subsequent transit times and durations, along with correct interpretation of TTVs within the system.

In this paper, we present a dynamical analysis of the Kepler-89 system, that includes stability tests for a variety of Keplerian orbital solutions and a study of the

effects of periastron precession. In Section 2 we review the architecture of the Kepler-89 system and calculate the Hill radii and mutual Hill radii separations for each of the planets. Section 3 provides the detailed results of an extended suite of stability simulations for the system, described in terms of the short-term stability (Section 3.1), long-term stability (Section 3.3), and the periastron precession effects (Section 3.4). The consequences of the precession effects are described in Section 4, particularly the impact on transit times and durations in comparison to TTV amplitudes. We conclude in Section 5 and detail relevance to other compact systems with suggestions for further work and observations.

2. ORBITAL ARCHITECTURE OF THE KEPLER-89 SYSTEM

The stellar and planetary properties required for the study presented here were extracted from Weiss et al. (2013), including the stellar mass of $M_\star = 1.277 \pm$

$0.050 M_\odot$. Since the argument and times of periastron are not provided by Weiss et al. (2013), we adopt periastron arguments of $\omega = 90^\circ$ (locations of inferior conjunction) and periastron times equivalent to the times of mid-transit provided by Weiss et al. (2013). Shown in Table 1 are the orbital period, P , eccentricity, e , minimum planet mass, $M_p \sin i$, semi-major axis, a , and Hill radius, R_H for each of the known planets. The orbital periods of planets c and d show that they are in near 2:1 resonance, which has implications for their orbital stability. The Hill radius is given by

$$R_H = r \left(\frac{M_p}{3M_\star} \right)^{1/3} \quad (1)$$

where r is Keplerian star-planet separation

$$r = \frac{a(1 - e^2)}{1 + e \cos f} \quad (2)$$

where f is the true anomaly. Since the Hill radius is time-dependent for a Keplerian orbit, the Hill radius shown in Table 1 is the mean Hill radius (where $r = a$).

Table 1. Kepler-89 Planetary Parameters

Parameter	b	c	d	e
P (days)	3.743208 ± 0.000015	10.423648 ± 0.000016	22.3429890 ± 0.0000067	54.32031 ± 0.00012
e	0.25 ± 0.17	0.43 ± 0.23	0.022 ± 0.038	0.019 ± 0.23
$M_p \sin i$ (M_\oplus)	10.5 ± 4.6	$15.6_{-15.6}^{+5.7}$	106 ± 11	35_{-28}^{+18}
a (AU)	0.05119 ± 0.00067	0.1013 ± 0.0013	0.1684 ± 0.0022	0.3046 ± 0.0040
R_H (10^{-3} AU)	1.03	2.33	7.36	9.18

The orbits of the planets are shown in Figure 1. As a first-order approximation for system stability, we use the mutual Hill radii between adjacent planet pairs:

$$R_{H,M_p} = \left[\frac{M_{p,in} + M_{p,out}}{3M_\star} \right]^{\frac{1}{3}} \frac{(a_{in} + a_{out})}{2} \quad (3)$$

where the “in/out” subscripts refer to the inner and outer planets in the system (Crossfield et al. 2015; Sinukoff et al. 2016). Gladman (1993) established a criterion for stability, requiring separation between planets in two-planet systems be larger than 3.5 mutual Hill radii. The criterion was extended by Smith & Lissauer (2009) to multi-planet systems by defining $\Delta = (a_{out} - a_{in})/R_H$ and requiring that $\Delta > 9$ for two adjacent planets, and $\Delta_{in} + \Delta_{out} > 18$ for three adjacent planets where Δ_{in} and Δ_{out} are the Δ calculations for the inner and outer adjacent planet pairs respectively. We modify Equation 3 to account for eccentricity with $(1 + e)$ and $(1 - e)$ multiplicative factors for a_{in} and a_{out} respectively.

For the Keplerian orbital solution shown in Table 1, we calculate $\Delta_{bc} + \Delta_{cd} + \Delta_{de} = 3.94 + 8.97 + 11.54 = 24.45$. This indicates that the Keplerian orbital solution is unstable as stated, particularly between planets b and c. If we assume circular orbits for all of the planets, we obtain $\Delta_{bc} + \Delta_{cd} + \Delta_{de} = 24.03 + 10.89 + 12.00 = 46.92$, indicating stability between pairs and overall system stability. These stability scenarios are tested in detail in the following section.

3. ORBITAL STABILITY AND PRECESSION EFFECTS

The orbital stability simulations described here were carried out using N-body integrations with the Mercury Integrator Package (Chambers 1999). We adopt a similar methodology to that used by Kane & Raymond (2014); Kane (2016), which systematically explored stability for ranges of orbital eccentricity and inclination. The dynamical simulations made used the hybrid

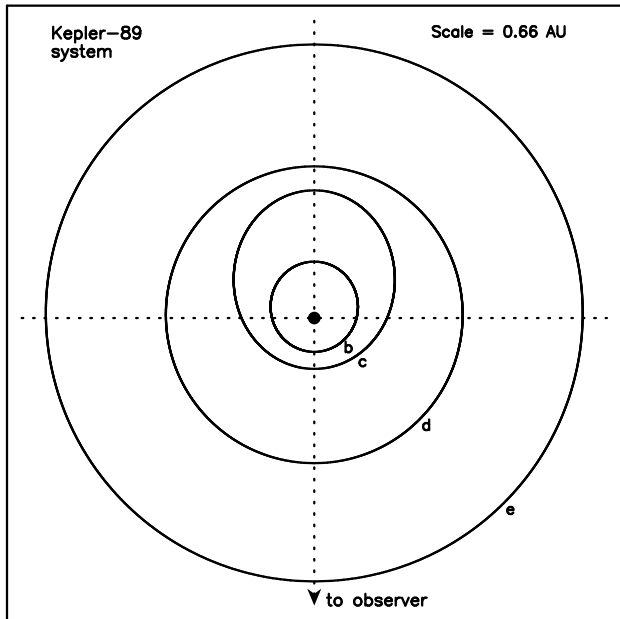


Figure 1. A top-down view of the Kepler-89 system, showing the host star (intersection of the dotted cross-hairs) and the orbits of the planets (solid lines). The Keplerian orbits are as described by the parameters in Table 1 with $\omega = 90^\circ$. The scale of the figure is 0.66 AU along one edge of the box.

symplectic/Bulirsch-Stoer integrator with a Jacobi coordinate system that generally provides more accurate results for multi-planet systems (Wisdom & Holman 1991; Wisdom 2006) except in cases of close encounters (Chambers 1999). We performed a variety of 10^6 and 10^7 year integrations commencing at the present epoch with the orbital configuration output every 100 simulation years. In accordance with the recommendations of Duncan et al. (1998), we set the time resolution to 0.1 days to meet the minimum required resolution of $1/20$ of the shortest orbital period within the system. We randomize the starting positions (mean anomalies) of the planets to create a robust snapshot of the orbital stability for the examined architecture. Stability of simulations may be evaluated via chaos indicators that measure the divergence of orbits, such as the criterion developed by Cincotta & Simó (1999, 2000) and applied to exoplanetary orbits (Goździewski et al. 2001; Goździewski 2002; Satyal et al. 2013, 2014). Our criteria for stability is a relatively simple first-order approach that requires all planets survive the duration of the dynamical simulation. This method is based on divergent orbital eccentricities which means that the planet has either been ejected from the system or succumbed to the host star. The simple stability criteria was compared with chaos indicators by Dvorak et al. (2010) and has been successfully applied to exoplanetary systems in numerous instances (Menou & Tabachnik 2003; Dvorak et al. 2003; Kane 2016). The additional details for the individual simulations are outlined below.

3.1. Short-Term Stability

Tests for the short-term stability of the system were conducted for 10^6 years with both the eccentric model (Table 1) and circular model ($e = 0.0$) parameters as input starting conditions. For the eccentric model, all simulations were found to be dramatically unstable, generally resulting in the inner (b) planet being removed from the system within the first several hundred years. The circular model remained stable for the full 10^6 year simulation in all cases and the eccentricities of the planets remained below 0.001 for planets b, d, e, and below 0.005 for planet c.

It is worth noting that the removal of planets does not necessarily mean that they are ejected from the system. Particularly for compact systems such as Kepler-89, it is non-trivial for inner planets to escape the gravitational potential well of the host star, resulting in the planets being consumed by the host star rather than ejected.

3.2. Near Resonance of Planets c and d

It was noted by Weiss et al. (2013) that planets c and d are in near 2:1 resonance. We investigated the extent to which the resonance scenario is true by executing a short-term (10^3 years) simulation that assumes circular orbits for all planets, and using a high-resolution (1 day) time output. To test for sustained resonance between the planets, we calculated the resonance angle using the methodology of Ketchum et al. (2013) and investigated both the short-term and long-term behavior of the c and d planetary orbits.

The results of the resonance analysis are encapsulated in Figure 2. The top panel shows the full 10^3 year variation of the resonance angle between planets c and d assuming a 2:1 resonance. The plot demonstrates that, although the planets are indeed close to the 2:1 secular resonance, they regular diverge from resonance and so do not permanently occupy the 2:1 resonance configuration in a stable fashion. The bottom panel is a zoomed in portion of the top panel during one of the periods of pseudo-resonance, during which the resonance angle of the planets oscillates with a peak-to-peak amplitude of $\sim 100^\circ$ for a period of ~ 80 years before the planets separate from resonance. We additionally investigated the resonance angle of the other planet pairs in the system but did not locate any resonant pairs.

3.3. Long-Term Stability

To investigate the long-term dynamical stability of the Kepler-89 system, we extended the duration of the N-body integrations with a variety of initial orbital architectures. The chosen duration of 10^7 years represents $\sim 10^9$ orbital periods of the inner planet and $\sim 6.7 \times 10^7$ orbital periods of the outer planet. For context, 10^7 years represents $\sim 4.2 \times 10^7$ orbital periods of Mercury

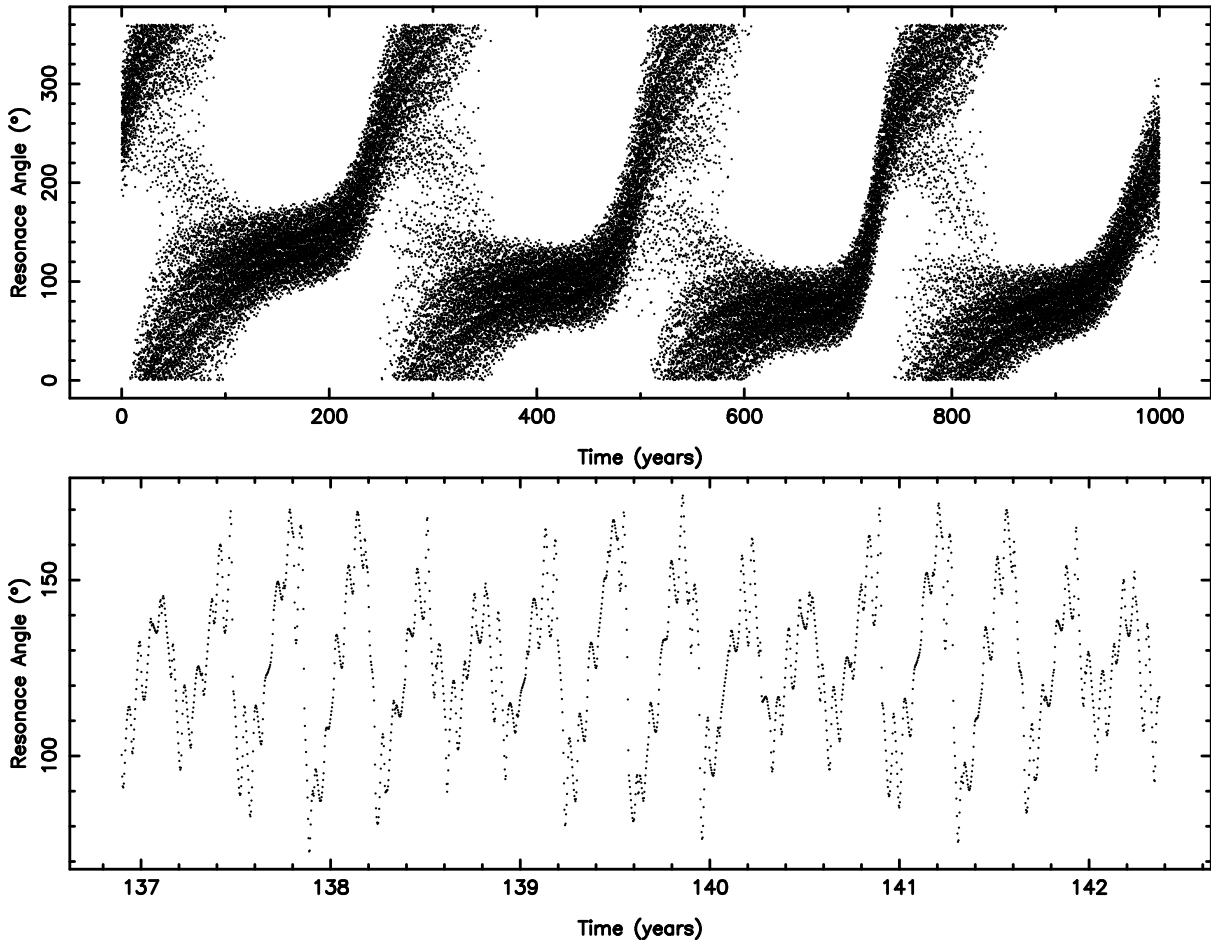


Figure 2. The resonance angle for planets c and d assuming circular orbits, as described in Section 3.2. Top panel: the results for the full 10^3 year simulation, demonstrating that the planets do not remain in a stable long-term 2:1 secular resonant configuration. Bottom panel: a zoomed version of the top panel for a period when the planets are in a short term 2:1 pseudo-resonance.

and $\sim 6.1 \times 10^4$ orbital periods of Neptune. Since it is the relative number of orbital periods that is used as a metric for time durations relative to orbital stability, 10^7 years is sufficient for a compact system such as Kepler-89.

An important aspect of the system architecture to note is that planet c is only $\sim 50\%$ more massive than planet b. However, the eccentricity of planet c is the primary cause of the system instability for the eccentric model of the system. For example, even if planet b begins in a circular orbit, whilst the other planets begin with the eccentricities shown in Table 1, then planet b is very quickly removed from the system due to the perturbing effects of planet c. The outcome of this simulation is depicted in the top panel of Figure 3, where the three remaining planets maintain long-term stability. The angular momentum loss from the removal of planet b results in a dampened eccentricity of planet c which is then periodically transferred to the two remaining outer planets. On the other hand, if planet c begins

in a circular orbit whilst all the other planets start with their measured eccentricities then the system is stable, shown in the bottom panel of Figure 3. Therefore we explored the eccentricities of planet c that allow system stability for at least 10^7 years. Hereafter, we refer to the eccentricities of planets b and c as e_b and e_c respectively.

In the case of the eccentric model and with planet b starting a circular orbit, the conducted simulations result in system stability for 10^7 years when $e_c \leq 0.26$. An example of this is shown in the top panel of Figure 4 where $e_b = 0.0$ and $e_c = 0.26$. As can be seen, planet b cannot remain in a circular orbit due to perturbation from the other planets. However, planets b and c maintain a stable configuration whilst transferring angular momentum to each other, except for a brief period at $\sim 1.5\text{--}3$ Myrs where planet e gains some angular momentum resulting in a slight increase in eccentricity.

As demonstrated in Section 3.1, the fully eccentric model of the system is highly unstable. We gradually decreased the eccentricity of planet c until long-term

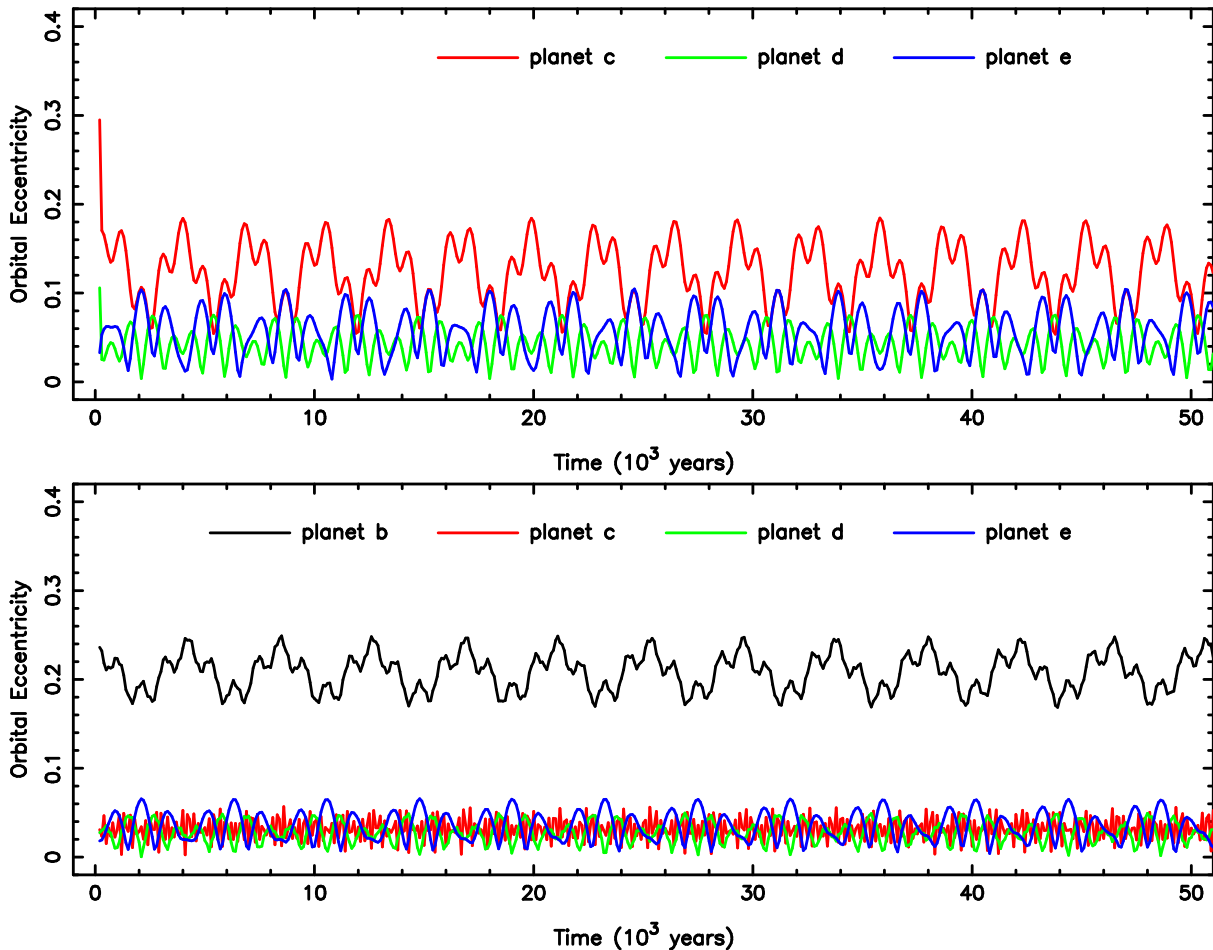


Figure 3. The eccentricity as a function of time for the four planets of the Kepler-89 system. Top panel: assuming an eccentric model with planet b starting in a circular orbit. Planet b is almost immediately ejected from the system (after less than 200 years), due to perturbations resulting from interactions with planet c. Bottom panel: assuming an eccentric model with planet c starting in a circular orbit. The system is able to maintain long-term stability in this case.

dynamical stability was achieved. We found that the eccentric model of the system is generally stable for 10^7 years when $e_c \leq 0.22$. An example of one of these simulations is represented in the bottom panel of Figure 4. It can be seen in the figure that a relatively chaotic exchange of angular momentum between planets b, c, and e commences after a simulation duration of ~ 5.5 Myrs. Planet d remains relatively unaffected by this sudden onset of momentum exchange due to its mass being substantially larger than the other three planets (see Table 1). A further aspect worth noting is that, even though the eccentric model of the system is unstable for $e_c > 0.22$, not all such simulations result in the loss of planet b. In some cases planet b survives whilst planet c is ejected. An example of this is when $e_c = 0.24$, in which case the planetary orbital dynamics result in the loss of planet c after ~ 1.5 Myrs. Recall that planet c is in a near 2:1 secular resonance with planet d (see Section 3.2), and the rare occasions when planet c loses its orbital integrity is because it has been pushed out

of the near 2:1 resonant island that provides temporary orbital stability (Agnew et al. 2019). Shown in Figure 5 is a summary plot of the variation of the starting eccentricity of planet c for the eccentric model, from 0.0 to 0.27, and the resulting stability of planets b and c. The stability is described as the percentage of the simulation time (10^7 years) for which each planet survived. Planets d and e are not shown in the plot since they survived in all of the cases encapsulated by the plot.

We further investigated the dynamical behavior of planets b and c for the eccentric model with a starting eccentricity of $e_c = 0.22$ (Figure 4, bottom panel) by calculating the trajectory of the apsidal modes. Detailed descriptions of apsidal motion in the context of interacting exoplanetary systems are provided by Barnes & Greenberg (2006b,a), where the two basic types of apsidal behavior, libration and circulation, are separated by a boundary called a secular separatrix (Barnes & Greenberg 2006a; Kane & Raymond 2014). The apsidal trajectories for planets b and c in

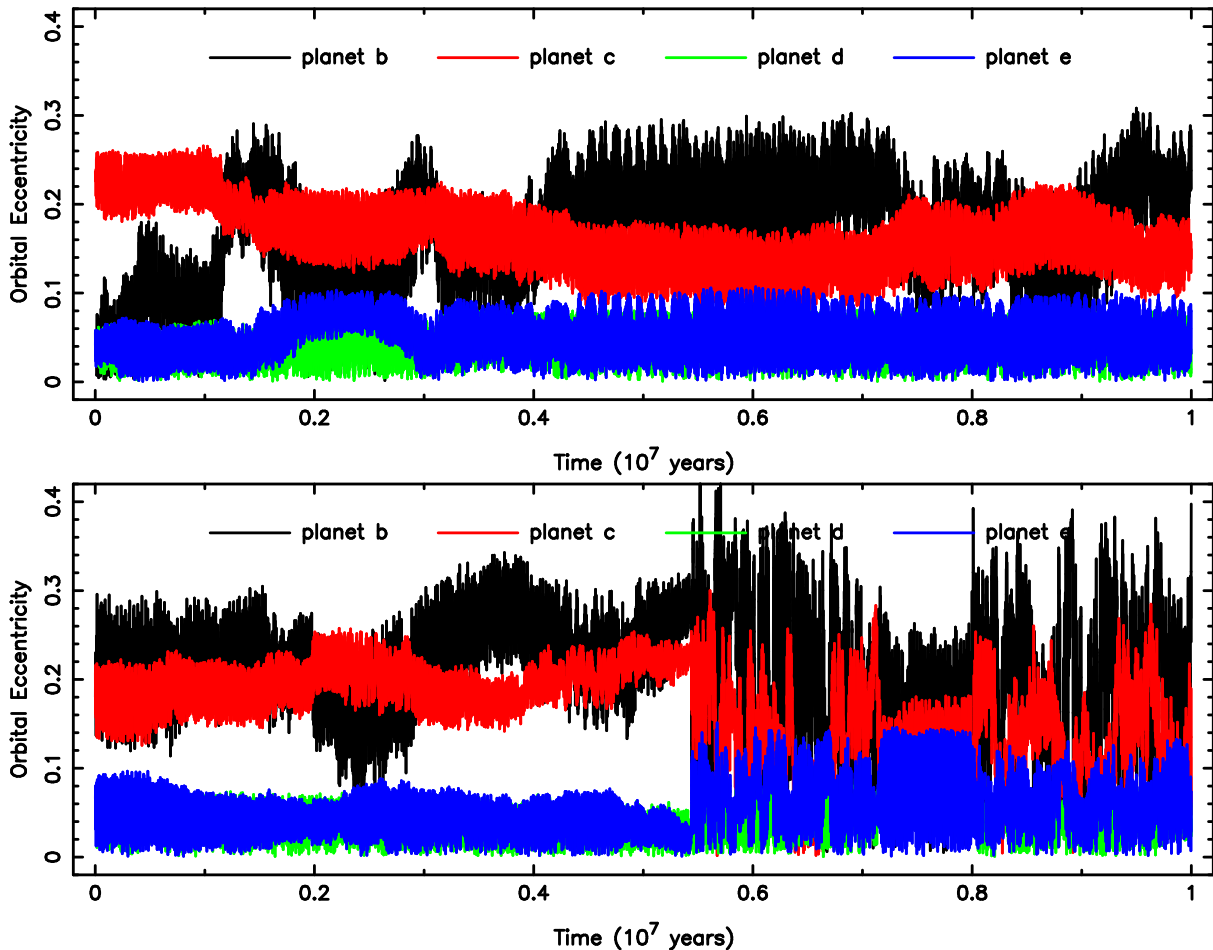


Figure 4. The eccentricity as a function of time for the four planets of the Kepler-89 system, where the system maintained stability for the full 10^7 year duration. Top panel: assuming an eccentric model with starting conditions for planets b and c of $e_b = 0.0$ and $e_c = 0.26$ respectively. Planets b and c exchange significant amounts of angular momentum but retain orbital integrity. Bottom panel: assuming an eccentric model with a starting eccentricity of $e_c = 0.22$. This represents the maximum allowed starting eccentricity for planet c in the fully eccentric model of the system for which long-term orbital stability is achieved.

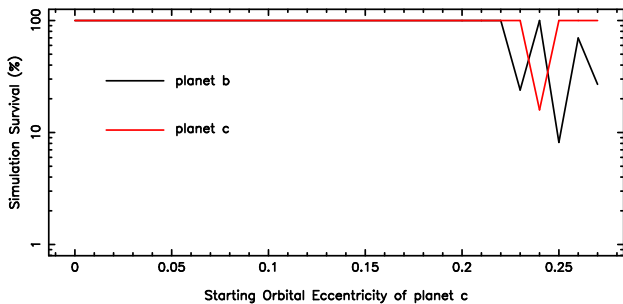


Figure 5. A summary plot of the starting eccentricities of planet c for the eccentric model and the resulting stability of planets b and c, expressed as a percentage of the total simulation time (10^7 years).

the Kepler-89 system are represented graphically in polar form in Figure 6. The time span over which these are shown are the first 2 Myrs of the simulation before the relatively chaotic transfer of angular momentum between the system planets occurs at ~ 5.5 Myrs. During

this stable period, Figure 6 shows that the planets are circulating since the polar trajectories consistently encompass the origin.

It was described in Section 2 that we adopted periastron argument values of $\omega = 90^\circ$ for all planets since these are not provided by the published orbital solutions and there is a vast number of possible combinations. The periastron arguments were assigned the same value to ensure that apastron for the planets occurs on the same side of the star, thus minimizing close encounters between the planets and optimizing the potential system stability. The previous paragraph described how the eccentric model is only stable where $e_c \leq 0.22$. We performed an additional test of stability by changing the argument of periastron for the inner planet to $\omega_b = 270^\circ$. As expected, this places more stringent constraints on the stable Keplerian orbital elements for the other planets. For this scenario using the eccentric model de-

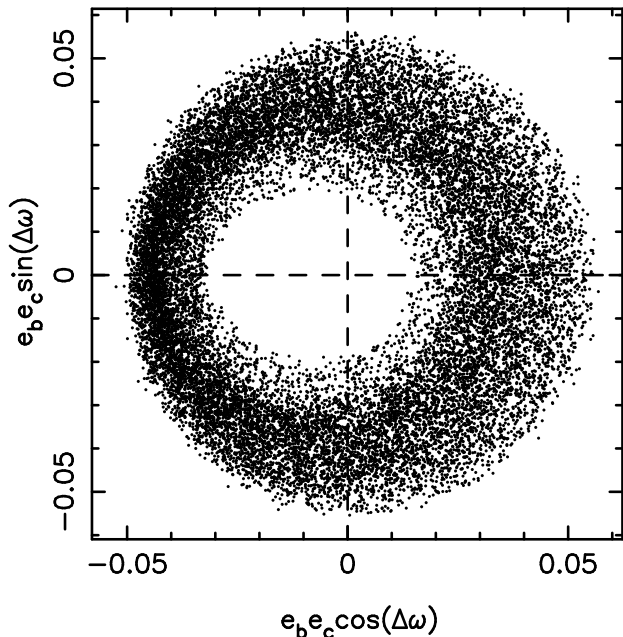


Figure 6. A polar plot of the apsidal trajectory ($e_b e_c$ versus $\Delta\omega$) for the b and c planets. These data represent the first 2 Myrs of the eccentric model with a starting planet c eccentricity of $e_c = 0.22$ (bottom panel of Figure 4). The figure shows that the apsidal modes are circulating during the initial ~ 5.5 Myrs of the simulation.

scribed above, system stability is only achieved for the full 10^7 years when $e_c \leq 0.19$.

Finally, we note that the eccentricity constraints presented in this section for the eccentric model are well within the eccentricity uncertainties for the system, shown in Table 1. The final example described in the previous paragraph retains the original eccentricities for planets b, d, and e and reduces the initial eccentricity of planet c to $e_c = 0.22$, compared with the value of $e_c = 0.43 \pm 0.23$ shown in Table 1.

3.4. Argument of Periastron Precession

The dynamical nature of compact planetary systems results in constant adjustments of the Keplerian orbits for each of the planets. One of the ways in which these adjustments are observed is through the precession of the orbital periastron arguments. As an example of the rate at which periastron precession can occur for the inner planets, we conducted a 10^6 year duration dynamical simulation with an output interval of 1 year in order to capture the rapid pace of periastron precession. This simulation was performed using the maximum eccentricity orbital architecture with $e_c = 0.22$, described in Section 3.3 and shown in the bottom panel of Figure 4. The precession described here includes the effects of both general relativity (GR) and perturbations of other planets (Bolmont et al. 2015).

The resulting rate of change in periastron over the first 10^4 simulation years are shown in Figure 7 for planet b

(top panel) and planet c (bottom panel). The orbits of both planets are subjected to significant periastron precession, with planet c having a much more rapid precession due to the combined influences of the surrounding planets. As can be seen in Figure 7, the rate of periastron precession is non-uniform, but the mean rate of precession over the 10^4 year simulation are $0.51^\circ/\text{year}$ and $1.76^\circ/\text{year}$ for planets b and c respectively. For comparison, the perihelion of Mercury precesses at a rate of $0.0119^\circ/\text{century}$ due to GR effects, and $0.148^\circ/\text{century}$ due to perturbations from other solar system planets (Clemence 1947; Iorio 2005). Thus the precession rates of the planets are relatively fast, possibly resulting in observable effects for future transit events.

4. EFFECT OF ORBITAL DYNAMICS ON TRANSITS

As described in Section 3.4, the inner planets of the Kepler-89 system undergo significant periastron precession, largely due to planet-planet perturbations. The effect of precession on transit times and duration has been studied by various authors (Miralda-Escudé 2002; Heyl & Gladman 2007; Jordán & Bakos 2008; Pál & Kocsis 2008; Ragozzine & Wolf 2009; Carter & Winn 2010; Damiani & Lanza 2011; Herman et al. 2018), and the additional impact on transit probabilities has been similarly quantified (Kane et al. 2012). Depending upon the system architecture, the effects of the periastron precession may be observable over a timescale less than a few years.

The Kepler-89 system has been subjected to several independent TTV analyses (Masuda et al. 2013; Xie et al. 2014; Holczer et al. 2016; Hadden & Lithwick 2017), including that of the discovery paper, Weiss et al. (2013). For example, Masuda et al. (2013) found that the TTVs for Kepler-89c have a semi-amplitude ~ 7 minutes and a period of ~ 155 days, caused mostly by the aforementioned near 2:1 resonance with planet d. The periastron precession rate of planet c described in Section 3.4 is sufficiently large that it can impact the calculation of the predicted transit observables. The precession rate of planet c in the eccentric model is $1.76^\circ/\text{year}$, or $0.05^\circ/\text{orbit}$. The net effect of this precession is to bring the predicted transit time forward by ~ 2 minutes/orbit. This effect is generally accounted for in TTV calculations and the observability of this effects may be utilized as an additional constraint upon eccentricity if it is not observed in the transit data.

Keplerian orbital elements can also have a significant effect on the duration of a planetary transit (Barnes 2007; Burke 2008). From Burke (2008), the duration

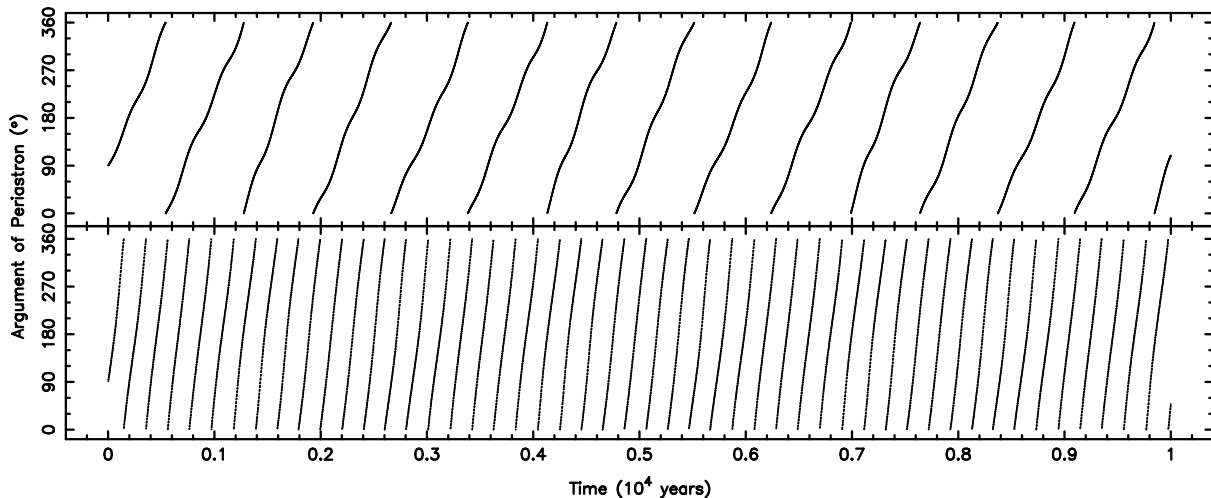


Figure 7. Depiction of periastron precession for planets b (top) and c (bottom) for the eccentric model described in the bottom panel of Figure 4. The precession rates for planets b and c are $0.51^\circ/\text{year}$ and $1.76^\circ/\text{year}$ respectively.

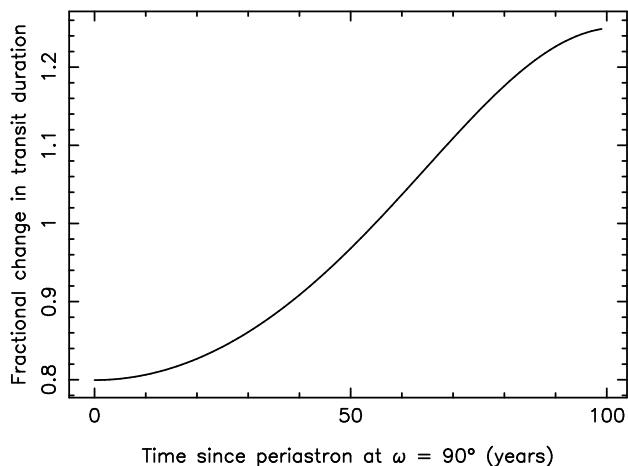


Figure 8. The fractional change in transit duration as a function of time (in years) since the periastron argument was located at $\omega = 90^\circ$.

of a transit scales according to the following relation:

$$\tau = \frac{\sqrt{1-e^2}}{1+e\cos(\omega-90^\circ)} \quad (4)$$

Combining this scaling relationship with periastron precession results in a time-dependent transit duration. For Kepler-89c, the rate of precession results in $\sim 180^\circ$ change in the argument of periastron over the course of 100 years. This is represented in Figure 8, where the fractional change in the transit duration is plotted against the time (in years) since the periastron argument was location at 90° . For the eccentricity of $e_c = 0.22$, the transit duration has a fractional change of ~ 0.4 between inferior and superior conjunction, or a fractional change of $0.004/\text{year}$ 1 part in 10,000 per orbit. Thus, although the effect of periastron precession on transit duration is unlikely to be detected between orbits, the effect could be reasonably observed with further transit

observations in subsequent years.

5. CONCLUSIONS

The orbital dynamics of compact planetary systems is a topic of crucial importance at the present time, since current detection methods are biased towards the detection of such systems and the extraction of reliable masses via TTVs is dependent upon the mutual interactions of the planets. Orbital stability in compact systems is exceptionally sensitive to the eccentricities of the individual planets, which in turn are difficult to measure for the majority of *Kepler* systems due to the relative faintness of the host star. The Kepler-89 system is an example of this, where the Keplerian orbital parameters are largely determined from the *Kepler* photometry rather than the RV data, whose utility is mostly to provide a mass estimate for the giant planet (planet d).

In this work, we have used the Kepler-89 system as a template from which it is demonstrated how the orbital eccentricity may be constrained through the use of dynamical simulations. The results presented here demonstrate that dynamical simulations may be used as a powerful tool to explore numerous possible dynamical architectures that result from systems. For example, we show that there is a limited range of eccentricities for planets b and c (e.g., $e_c \leq 0.22$ for the fully eccentric model) that ensure long-term dynamical stability, and we have shown how the eccentricities vary with time for several of the stable orbital architectures. We have further demonstrated the dramatic periastron precession that may be occurring within the Kepler-89 system; a result of both the compact architecture combined with eccentricities that lie at the upper boundaries of stability. The periastron precession for Kepler-89c is significant enough that it should result in observable effects,

or else rule out the eccentricity that would produce such precession. In either case, the precession effects should be carefully considered when performing accurate transit timing and duration measurements.

The near 2:1 secular resonance of planets c and d is an important aspect of the overall system architecture, and particularly important since planet d is the dominant planetary mass in the system. As shown in Section 3.2, planets c and d are not quite in resonance but occasionally exhibit resonant behavior. A 2:1 secular resonance would raise the question of whether the system could dynamically harbor a three-body Laplace resonance with a 4:2:1 orbital period ratio. There are several known examples of Laplace resonances among exoplanetary systems, such as GJ 876 (Rivera et al. 2010), Kepler-60 (Goździewski et al. 2016), and TRAPPIST-1 (Luger et al. 2017). It was also proposed by Libert & Renner (2013) that Laplace resonances could be detected via long-term observations of TTV effects. In order for Kepler-89 to contain such a resonance that extends the existing near 2:1 secular resonance of planets c and d to a Laplace configuration, an additional planet would need to be located close to either a 5 day or 44 day orbital period. Given the relatively tenuous stability of the b and c planets and the high mass of the d and e planets, such a Laplace resonance may be difficult to achieve, but nonetheless important for future observers of the system to keep in mind.

Many uncertainties remain in the Keplerian orbital elements of the Kepler-89 system that will require further RV observations and/or precise transit times to resolve. However, the compact nature of the system combined with the possibility of non-zero eccentricities

make the system a good case-study for exploring the dynamical effects of the orbits on each other and observable effects. The dynamical effects include gravitational perturbations, precession of orbits, mean motion resonances, and secular resonances. Strategies for the refinement of planetary orbits are being applied to numerous known exoplanetary systems (Kane et al. 2009), and could be further applied to systems that are predicted to produce similar observable signatures. It is possible that the time baseline of *Kepler* observations is too short to observe the discussed precession effects, but observations of the *Kepler* field by the Transiting Exoplanet Survey Satellite (*TESS*) may sufficiently extend the baseline to reveal eccentricities hidden in the photometry.

ACKNOWLEDGEMENTS

The author would like to thank Lauren Weiss for several insightful discussions regarding the Kepler-89 system, and also Rory Barnes, Paul Dalba, Sean Raymond, and Paul Wiegert for useful feedback on the manuscript. Thanks are also due to the anonymous referee, whose comments greatly improved the quality of the paper. This research has made use of the following archives: the Habitable Zone Gallery at hzgallery.org and the NASA Exoplanet Archive, which is operated by the California Institute of Technology, under contract with the National Aeronautics and Space Administration under the Exoplanet Exploration Program. The results reported herein benefited from collaborations and/or information exchange within NASA's Nexus for Exoplanet System Science (NExSS) research coordination network sponsored by NASA's Science Mission Directorate.

Software: Mercury (Chambers 1999)

REFERENCES

- Agnew, M. T., Maddison, S. T., Horner, J., & Kane, S. R. 2019, *MNRAS*, 485, 4703
- Barnes, J. W. 2007, *PASP*, 119, 986
- Barnes, R., & Greenberg, R. 2006a, *ApJ*, 652, L53
- . 2006b, *ApJ*, 638, 478
- Bolmont, E., Raymond, S. N., Leconte, J., Hersant, F., & Correia, A. C. M. 2015, *A&A*, 583, A116
- Borucki, W. J. 2016, *Reports on Progress in Physics*, 79, 036901
- Borucki, W. J., Koch, D., Basri, G., et al. 2010, *Science*, 327, 977
- Burke, C. J. 2008, *ApJ*, 679, 1566
- Carter, J. A., & Winn, J. N. 2010, *ApJ*, 716, 850
- Chambers, J. E. 1999, *MNRAS*, 304, 793
- Cincotta, P., & Simó, C. 1999, *Celestial Mechanics and Dynamical Astronomy*, 73, 195
- Cincotta, P. M., & Simó, C. 2000, *A&AS*, 147, 205
- Clemence, G. M. 1947, *Reviews of Modern Physics*, 19, 361
- Crossfield, I. J. M., Petigura, E., Schlieder, J. E., et al. 2015, *ApJ*, 804, 10
- Damiani, C., & Lanza, A. F. 2011, *A&A*, 535, A116
- Duncan, M. J., Levison, H. F., & Lee, M. H. 1998, *AJ*, 116, 2067
- Dvorak, R., Pilat-Lohinger, E., Funk, B., & Freistetter, F. 2003, *A&A*, 410, L13
- Dvorak, R., Pilat-Lohinger, E., Bois, E., et al. 2010, *Astrobiology*, 10, 33
- Funk, B., Wuchterl, G., Schwarz, R., Pilat-Lohinger, E., & Eggl, S. 2010, *A&A*, 516, A82
- Gladman, B. 1993, *Icarus*, 106, 247
- Goździewski, K. 2002, *A&A*, 393, 997
- Goździewski, K., Bois, E., Maciejewski, A. J., & Kiseleva-Eggleton, L. 2001, *A&A*, 378, 569
- Goździewski, K., Migaszewski, C., Panichi, F., & Szuszkiewicz, E. 2016, *MNRAS*, 455, L104
- Granados Contreras, A. P., & Boley, A. C. 2018, *AJ*, 155, 139
- Hadden, S., & Lithwick, Y. 2017, *AJ*, 154, 5
- Herman, M. K., de Mooij, E. J. W., Huang, C. X., & Jayawardhana, R. 2018, *AJ*, 155, 13
- Heyl, J. S., & Gladman, B. J. 2007, *MNRAS*, 377, 1511
- Holzer, T., Mazeh, T., Nachmani, G., et al. 2016, *ApJS*, 225, 9
- Holman, M. J., Fabrycky, D. C., Ragozzine, D., et al. 2010, *Science*, 330, 51

- Howell, S. B., Sobek, C., Haas, M., et al. 2014, *PASP*, 126, 398
- Iorio, L. 2005, *A&A*, 433, 385
- Jordán, A., & Bakos, G. Á. 2008, *ApJ*, 685, 543
- Kane, S. R. 2015, *ApJL*, 814, L9
- . 2016, *ApJ*, 830, 105
- . 2017, *ApJL*, 839, L19
- Kane, S. R., Horner, J., & von Braun, K. 2012, *ApJ*, 757, 105
- Kane, S. R., Mahadevan, S., von Braun, K., Laughlin, G., & Ciardi, D. R. 2009, *PASP*, 121, 1386
- Kane, S. R., & Raymond, S. N. 2014, *ApJ*, 784, 104
- Kane, S. R., & von Braun, K. 2008, *ApJ*, 689, 492
- Ketchum, J. A., Adams, F. C., & Bloch, A. M. 2013, *ApJ*, 762, 71
- Libert, A.-S., & Renner, S. 2013, *MNRAS*, 430, 1369
- Lissauer, J. J., Fabrycky, D. C., Ford, E. B., et al. 2011, *Nature*, 470, 53
- Lissauer, J. J., Jontof-Hutter, D., Rowe, J. F., et al. 2013, *ApJ*, 770, 131
- Luger, R., Sestovic, M., Kruse, E., et al. 2017, *Nature Astronomy*, 1, 0129
- Masuda, K., Hirano, T., Taruya, A., Nagasawa, M., & Suto, Y. 2013, *ApJ*, 778, 185
- Menou, K., & Tabachnik, S. 2003, *ApJ*, 583, 473
- Miralda-Escudé, J. 2002, *ApJ*, 564, 1019
- Pál, A., & Kocsis, B. 2008, *MNRAS*, 389, 191
- Quarles, B., Quintana, E. V., Lopez, E., Schlieder, J. E., & Barclay, T. 2017, *ApJL*, 842, L5
- Ragozzine, D., & Wolf, A. S. 2009, *ApJ*, 698, 1778
- Rivera, E. J., Laughlin, G., Butler, R. P., et al. 2010, *ApJ*, 719, 890
- Satyral, S., Hinse, T. C., Quarles, B., & Noyola, J. P. 2014, *MNRAS*, 443, 1310
- Satyral, S., Quarles, B., & Hinse, T. C. 2013, *MNRAS*, 433, 2215
- Sinukoff, E., Howard, A. W., Petigura, E. A., et al. 2016, *ApJ*, 827, 78
- Smith, A. W., & Lissauer, J. J. 2009, *Icarus*, 201, 381
- Weiss, L. M., Marcy, G. W., Rowe, J. F., et al. 2013, *ApJ*, 768, 14
- Winn, J. N., & Fabrycky, D. C. 2015, *ARA&A*, 53, 409
- Wisdom, J. 2006, *AJ*, 131, 2294
- Wisdom, J., & Holman, M. 1991, *AJ*, 102, 1528
- Xie, J.-W., Wu, Y., & Lithwick, Y. 2014, *ApJ*, 789, 165